Multiplexed, UVC-Induced, Sequence-Dependent DNA Damage Detection

*Sindhu G. Nair and Glen R. Loppnow**

Department of Chemistry, University of Alberta, Edmonton, Alberta T6G 2G2, Canada

*To whom correspondence should be addressed
Email: glen.loppnow@ualberta.ca
Phone: (780) 492-9704
Fax: (780) 492-8231

Abstract

The exposure of DNA to ultraviolet (UV) radiation causes sequence-dependent damage. Thus, there is a need for an analytical technique that can detect damage in large numbers of DNA sequences simultaneously. In this paper, we have designed an assay for UVC-induced DNA damage in multiple oligonucleotides simultaneously by using a 96-well plate and a novel automated sample mover. The UVC-induced DNA damage is measured using smart probes, analogues of molecular beacons in which guanosine nucleotides act as the fluorescence quencher. Our results show that the oligonucleotide damage constants obtained with this method are reproducible and similar to those obtained in cuvettes. The calibration curve for poly-dT shows good linearity ($R^2 = 0.96$), with limits of detection (LOD) and quantification (LOQ) equal to 55 nM and 183 nM, respectively. The results show that the damage kinetics upon irradiation is sensitive to the different types of photoproducts formed in the different sequences used; i.e. poly-A oligonucleotides containing guanine are damaged at a faster rate than poly-A oligonucleotides containing either thymine or cytosine. Thus, detecting DNA damage in a 96-well plate and quantifying the damage with smart probes is a simple, fast and inexpensive mix-and-read technique for multiplexed, sequence-specific DNA damage detection.

Introduction

DNA damage leads to cancer, aging and other inheritable diseases (1). The major sources of DNA damage are ionizing radiation, UV radiation and chemicals. High levels of DNA damage (1) occur from exposure to UV radiation which extends from the UVA band (315-400 nm) through the UVB band (280-315 nm) and to the UVC band (190-280 nm). The primary products of DNA damage due to UV radiation are the pyrimidine dimers such as cyclobutane pyrimidine dimers (CPDs) and [6-4] pyrimidine pyrimidinone photoproducts ([6-4] PPs), as well as uracil and thymine photohydrates (2-4). In addition, oxidative damage may lead to the formation of 8-oxo-7, 8-dihydro-2'-deoxyguanosine (8-oxodGuo) (5) and other products, such as oxidized pyrimidine bases and DNA-protein crosslinks.

Studies shows that tumor genes contain multiple hotspots of damage and that these hot spots are sequence specific (6-10). Various computational (7) and statistical approaches (11) have been introduced to study the hot spots of mutation in human genome. Recently, a permutation-based study of the melanoma exome to look at mutations caused by UV light exposure led to the discovery of six novel melanoma genes (12). Thus there is a need for simple methods that can detect the hot spots of DNA damage in human genome.

A number of techniques have been used to detect DNA damage, including the polymerase chain reaction (PCR) (13,14), HPLC/MS-MS (15-17), GC-MS (18), gel electrophoresis (19), ^{32}P-postlabeling-HPLC assays (20) and various immunoassays (21). Though all the methods mentioned above have their advantages, they all involve the isolation and pre-purification of the damaged DNA. This separation is time consuming, expensive and may introduce additional lesions.

The development of fluorescence-based methods, such as molecular beacons (22), has introduced a new class of nucleic acid probes for DNA and DNA damage. Molecular beacons (MBs) are dual-labelled DNA hairpins with a fluorescent dye at one end and a fluorescence quencher at the opposite end. The MB is designed such that in the absence of target, the 3' and 5' ends self-hybridize, forcing the beacon to adopt a stem-loop structure and bringing the fluorophore and quencher into close

proximity. This arrangement quenches the fluorescence and no signal is observed. Upon hybridization of the MB loop to the complementary DNA target, however, the stem unwinds, forcing the fluorophore and quencher far apart and restoring the fluorescence (23-30). MBs have rapidly found applications in single-base pair mismatch measurements because of their high sensitivity and selectivity.

Increased knowledge about DNA damage and its direct link to cancer drives an urgent need for an analytical technique which is not only selective and sensitive but can detect damage in a large number of sequences simultaneously. But to study UV irradiation of ssDNA *in vitro* followed by its detection using MBs, a typical experiment involves the irradiation of each sample under study in a cuvette (22,31-33). Major limitations of this latter assay are that only a few samples can be done simultaneously and it is time consuming.

In this study, DNA damage susceptibility in four sequences is measured simultaneously with the high-throughput of a 96-well plate. To assay the DNA damage quantitatively, analogues of MBs called smart probes are used. These smart probes (SPs) use multiple guanines as the fluorescence quencher (33-36). Also, an automated remote well-plate mover is used to control the damage dose received by each sample. Thus our method can be used to construct a library of hot spots of DNA damage in different genomic sequence. The results obtained showed that this platform for inducing and detecting ssDNA damage compares favourably and quantitatively with cuvette-based methods.

Experimental

Materials. The SPs, MB and single-stranded oligonucleotide targets were obtained from Integrated DNA Technologies Inc. (Coralville, IA, USA). The sequences of the SPs, MB and target oligonucleotides used for this study are listed in Table 1. The target oligonucleotides were purified by standard desalting whereas the SPs and MB were purified by HPLC. MBs and SPs were designed to have stem melting temperatures ~5 °C higher than the hybrid melting temperatures.

UV Irradiation. Oligonucleotides were dissolved in nanopure water and the SPs and MB were dissolved in Tris buffer (10 mM Tris, 1 mM EDTA, pH ~7.4). All samples were kept frozen at -20^{o}C until needed. Upon thawing, the oligonucleotides were diluted to the required concentration in nanopure water. The MB and SPs were diluted in Tris buffer and annealed each time they were diluted. 100 µL of 1.6 µM nitrogen-purged samples of all four target sequences were placed in a 96-well plate (Corning Special Optics, NY, USA). UV light from UVC lamps emitting at 254 nm was chosen for the irradiation. The UVC light was turned on for 20 min prior to the experiment to ensure a stabilized light source. The photoreactor was purged continuously with nitrogen to remove oxygen and minimize ozone generation from the lamps. Finally, the 96-well plate was placed inside the remote plate mover (RPM) and positioned inside the Luzchem (Ottawa, ON, Canada) DEV photoreactor. Each well was exposed to UVC light for a specified time. Control samples were handled under identical condition, but were not exposed to UVC light.

The RPM is a custom-built device designed specifically for multiplexed irradiation experiments and can hold a maximum of two 96-well plates. The electronic control panel has 10 different time regulators, each of which can regulate time between 0.5 - 256 min. After the sample plates were positioned in the RPM, each row of the 96-well plate was set to a different exposure time. After irradiation, the 96-well plates were taken out of the RPM and the respective SPs were added to each well. The final concentration of the targets and SPs were made to 0.53 µM and 0.18 µM, respectively, by adding buffer (10 mM Tris, 1 mM EDTA, 5 mM $MgCl_2$, and 20 mM NaCl, pH ~7.4). The well plates were then incubated for 20 h in the dark at room temperature. For sensitivity measurements, 13.3 µl aliquots of dT_{17} sample were taken from 8 µM of irradiated solution in a cuvette at different time intervals and mixed with the appropriate amount of the probe and buffer to give a final concentration of 0.53 µM target and 0.18 µM complementary SP. These solutions were incubated in the dark for 20 h at room temperature and fluorescence spectra were recorded as described below.

Chemical Actinometry. Potassium iodide-iodate actinometry was performed to measure the number of photons absorbed by the irradiated cuvettes and well-plates. A solution consisting of 0.1 M KIO_3, 0.6 M KI and 0.01 M borate buffer at pH 9.25 was prepared as described by Rahn (37). The solution was placed in both a sealed, 1 cm pathlength UV-transparent cuvette (3 mL) and at twice the cuvette solution concentration in a 96-well plate (100 µL) within the photoreactor and irradiated with UVC light simultaneously under conditions identical to the UV irradiation of the DNA. The samples were exposed to radiation from four UVC lamps placed above the samples. The absorbance measurements before and after irradiation were made using a Hewlett-Packard (Sunnyvale, California) 8452A diode array spectrophotometer.

Fluorescence and absorbance measurements. Room-temperature fluorescence intensities were measured using the Safire fluorescence plate reader (Tecan, Mannendorf, Switzerland) for 300 µl of the hybridization mixture in the 96-well plate, containing 0.53 µM target and either 0.18 µM SP or MB in buffer. Fluorescence emission spectra were recorded using an excitation wavelength of 480 nm and an emission wavelength of 520 nm. The bandwidth for excitation and emission were 10 and 12 nm, respectively.

The SPs were characterized by their melting curve (22), in which temperature-dependent fluorescence measurements are carried out on buffered solutions of SPs incubated in the presence and absence of their complementary targets. These melting curves were also measured on solutions of SPs with irradiated target. The temperature was varied from 20°C to 80°C in increments of 4°C, a heating rate of 1°C/min and a 5 min settling time. Fluorescence spectra were measured using a Photon Technologies International (Birmingham, New Jersey) fluorescence system. The excitation wavelength was fixed at 480 nm and the emission was recorded from 490 to 700 nm (see Figure S1, Electronic Supplementary Material). The bandwidth for both excitation and emission were set at 4 nm. A 10 mm path length Suprasil quartz fluorescence cuvette was used for these measurements. Both melting and cooling curves were measured for all four SPs and their complementary targets, with SP concentrations

of 0.18 μM and target concentration of 0.53 μM. Absorbance measurements were performed on a Hewlett-Packard (Sunnyvale, California) 8452A diode array spectrophotometer.

Results and Discussion

In this paper, a method for simultaneously assaying the damage to a large number of single-stranded oligonucleotide samples was devised using a 96-well plate. All four oligonucleotide targets were irradiated in a 96-well plate and the resulting damage was measured by fluorescence. The damage constants obtained were compared with those obtained by the cuvette method.

Characterization of the Smart Probes. All the SPs used in this study were designed carefully to get the maximum performance as sensitive probes for DNA damage. A maximum discrimination between the SP and the SP-target hybrid for all the different sequences were obtained for a buffer with 10 mM Tris, 1 mM EDTA, 5 mM $MgCl_2$ and 20 mM NaCl, pH~7.4 (see Figure S4, Electronic Supplementary Material) and for an optimum working ratio between the SP and the target of 1:3 (see Figure S3, Electronic Supplementary Material). All the SPs used in this study were carefully designed to optimize their performance in selectively discriminating damage in the target oligonucleotides. The melting curves for all the SPs, in the absence and presence of complementary target oligonucleotide, are shown in Figure 1. It can be seen from the figure that the SPs exist in the hairpin form at low temperature and exhibit minimal fluorescence intensity. At these temperatures, the guanine residues at the 3′ end are in close proximity to the dye, quenching its fluorescence. As the temperature increases, the stem begins to melt, forcing the quenching guanosine residues farther from the fluorophore and resulting in higher fluorescence intensity (22,23,33). Finally at temperatures higher than 60°C, we saw a decrease in fluorescence with increasing temperature, since the fluorescence quantum yield of FAM decreases with increasing temperature.

In the presence of the perfectly complementary oligonucleotide target, a different pattern was seen for the melting curve. The hybrid melting curve starts with high fluorescence intensity due to the open form of the SPs, and gradually the fluorescence decreases until the target completely melts away from the hairpin probe. The hairpin probe reforms its stem-loop structure exhibiting low fluorescence intensity and, with the further increase in the temperature, gives the intermediate, high temperature fluorescence intensity of the SP-alone melting curve.

Similar patterns to the hybrid melting curves were obtained when the melting curves were plotted for the damaged oligonucleotide target-SP hybrids (Figure 1). As expected, the binding for the hybrid should be destabilized upon damaging the target sequence. For all the melting curves between the SPs and the damaged oligonucleotide targets in Figure 1, the hybrid has a lower fluorescence signal at low temperatures than the hybrid with the undamaged oligonucleotide. Also, the apparent melting temperature (T_m) of the damaged oligonucleotide target-SP hybrid is lower than that of the undamaged oligonucleotide target-SP hybrid. From Figure 1B, if we compare the melting temperatures between the damaged and undamaged TarG-SP_{TarG} hybrids, we find that the melting temperature decreases from 40^{o}C to 32^{o}C upon 88 min damage.

This hybrid stability in the presence and absence of damage can be correlated to the amount of damage. Figure 2 shows the melting curve for the SP_{dT17} alone and in the presence of irradiated dT_{17} at different time intervals. With the increase in the exposure time, the fluorescence melting curve is lower, indicating increasing damage. In addition, the T_m of the damaged target-SP hybrid also decreases with increasing irradiation time. This result shows that the SP is able to discriminate between different amounts of damage caused by UVC radiation. Similar results were obtained for the other targets.

DNA damage. The selectivity of SP to detect UVC-induced damage in oligonucleotide target dT_{17} was compared with that of the MB in a 96-well plate. The sequence of the MB used in this study is listed in Table 1. Similar to the SP, the MB has a fluorescein (FAM) fluorophore at the 5′ end but the guanine quencher is replaced by a dabcyl (DAB) quencher at its 3′ end. The decrease in the MB and SP

fluorescence intensity for dT_{17} target with increasing irradiation is shown in Figure 3. The damage constant obtained for the SP was 1.6 fold higher than the MB probe. The higher value of the damage constant indicates the lower the selectivity of the probe to detect damage. Thus, we can conclude that the selectivity of SP toward detecting UV damage is slightly less than that of the MB. This may be due to inefficient quenching of fluorescence by the guanosine residues (33) as depicted by its higher residual fluorescence.

To study the sensitivity of the SP for UVC-induced photoproducts, a dT_{17} target was chosen because of its well known photochemistry. The primary photoproducts of this target are thymine CPDs along with lower yields of [6-4] PPs and the Dewar isomer, in the ratio of 77:20:0.8 (2). To quantify the amount of photoproduct formed in this experiment, the absorbance of dT_{17} at 260 nm was measured as a function of irradiation time in a cuvette (see Figure S2, Electronic Supplementary Material). This absorbance band gradually bleaches with increasing irradiation time due to the loss of C_5=C_6 bond during the formation of thymine photoproducts. To confirm that the bleaching is only due to thymine photoproduct formation, the absorbance at 260 nm of the unirradiated control was also taken. Thus, the absorbance peak measured at 260 nm at different irradiation times is the weighted average of all three photoproducts formed (38). Figure 4 shows the calibration curve obtained by plotting the SP fluorescence as a function of calculated total concentration of photoproducts obtained from the absorbance measurements. At a zero concentration of photoproduct, the target is a perfect complement to the SP and gives maximum fluorescence intensity. As the amount of photoproduct increases up to 10 x 10^{-7} M, there is no considerable change in the fluorescence intensity, indicating that the SP has a threshold for the detection of DNA damage. Since the target concentration is 5.4 x 10^{-7} M and the threshold is 10 x 10^{-7} M, approximately 2-3 lesion sites on each target strand are necessary before the SP-target hybrid is destabilized enough to show a fluorescence decrease. This compares favourably to the 3-4 lesion necessary for the MB (22).

With a further increase in concentration of photoproduct, the fluorescence intensity decreases rapidly, showing the sensitivity of the SP toward DNA damage (Figure 4). The linear drop of fluorescence with increasing amount of photoproduct formation is shown more clearly in the inset of Figure 4. The calibration curve in this region shows good linearity with a linear regression coefficient of 0.96 and sensitivity (slope of the calibration curve) of 4.0 x 10^{11} M^{-1}. The resulting limit of detection (LOD) and limit of quantification (LOQ) values are therefore 55 nM and 183 nM, respectively. The standard deviation of the background used for the above calculation was obtained by measuring the fluorescence intensity of unhybridized SP samples (see Table S1, Electronic Supplementary Material).

Detection of UV-induced DNA photodamage in 96-well plate. Oligonucleotide solutions of all four sequences from Table 1 were irradiated in a 96-well plate at constant temperature and the damage constants for each sequence were obtained (Figure 5). The maximum irradiation time available in order to ensure that short-time kinetics were captured adequately was 248 min. By this time, the SP fluorescence intensity for all four target oligonucleotide had decreased to close to the intensity of SP alone. However, the lack of many points along the baseline means that the resulting time constants may have somewhat larger errors as a result. The damage constants along with their standard deviations are listed in Table 2.

The damage constants obtained in this study for TarC and TarT are 130 ± 40 min and 90 ± 10 min, respectively. Previous studies have shown that exposure of DNA containing adjacent pyrimidines, to UVC irradiation gives the CPD as the main photoproduct, with [6-4] PP and the Dewar isomers as the minor products (2). But the quantum yield for formation of photoproducts between adjacent thymines is larger than that for adjacent cytosines (39). The results obtained in this study clearly support the fact that thymine nucleobases are a preferential target for UVC-induced damage compared to cytosine.

The damage constants obtained for dT_{17} and TarT are 12 ± 0.7 min and 90 ± 10 min, respectively. As discussed above, the CPD is one of the major photoproducts formed between adjacent thymines. Therefore the ratio of formation of CPD photoproducts between dT_{17} and Tar T should be 8: 1, based on

198 the ratio of possible TT pairs that could form CPDs. Thus, we expect the damage constant for Tar T to
199 be 8 times slower than dT_{17}, consistent with the observed results.
200 The damage constant obtained for TarG in this study is 60 ± 10 min, which is surprisingly faster than
201 that of TarT. The major photoproduct of guanine in DNA is the formation of 8-oxodGuo, which has a
202 very low photoproduct formation rate (40). In both TarG and TarT sequences, the 'GG' and 'TT'
203 nucleobases have adenine as their neighbouring groups. Thus, there is a possibility of forming various
204 photoproducts. Previous studies (41,42) have shown that UVC irradiation of DNA strand containing
205 'AATTAA' would produce the AA and TA photoproducts, along with the CPD and [6-4] PP. However,
206 the AA and TA photochemical yields are at most only 10% those of TT, making these products much
207 less probable (43,44). The yield of formation of the [6-4] PP was found to have a sequence-dependent
208 photochemistry. However, in the case of guanine, UVC excitation may produce guanine radical cations
209 followed by 8-oxodGuo formation (45). Thus, the selectivity of the SP to detect damage will depend on
210 the change in conformation of the nucleobases upon photoproduct formation, and the 8-oxo-dG
211 photoproduct may be more disruptive to SP hybridization.
212 This discrepancy in the damage rates of TarT and TarG may also be attributed to the difference in
213 damage kinetics of the sequences due to the neighbouring nucleobases. In a previous experiment (46)
214 designed to study the reactivity of a TT dinucleotide embedded in different sequences, it was shown that
215 the rate of formation of thymine photoproduct is surprisingly slowed when the neighbouring groups are
216 changed from cytosines to adenines. It was assumed that the thymine nucleobases could be locked
217 between the neighbouring adenine residues, hindering the CPD photoproduct formation (46). Not much
218 work has been done to study the neighbouring group effect of the adenine nucleobases on the stability of
219 guanine radical cation.
220 The above arguments are true for highly homologous sequences. Despite the advantages of SP as a
221 general and inexpensive probe to detect DNA damage, SPs have the disadvantage of not being a very
222 selective probe for different types of DNA damage products. Thus, they may respond differently to

different damage products, either due to different kinetics or different binding constants of hybridization to targets with different positions or types of lesions. In addition, smart probes suffer from inefficient quenching by the guanosine residues, leading to a constant, non-zero background fluorescence and subsequently lower sensitivity. We are currently developing and characterizing probes with better sensitivity and selectivity than smart probes (31, 38).

Also, a comparative study of the damage constant obtained by the 96-well plate experiment was done with that of the cuvette experiments. Both methods gave the highest damage constant value for TarC and the lowest value for dT_{17}, supporting the fact that oligonucleotide dT_{17} has much faster rate of photoproduct formation when compared to the other three targets. However, the actual damage constants obtained in the cuvette experiments are all lower than the 96-well plate experiments as shown in Table 2. This change is due to the difference in the experimental conditions. When the experiments are performed in the cuvette, the samples are constantly stirred and subjected to a power of 220 mW from the UVC lamp, calculated from their irradiance and the geometry of irradiation. But for the 96-well plate experiments the power received by the unstirred samples in the wells is calculated to decrease to 2.6 mW. Similar ratios were obtained when iodide- iodate chemical actinometry (37) was performed on the cuvette and 96-well plate. The formation of triiodide was calculated from the increase in absorbance at 352 nm with increasing irradiation time. A calibration curve is obtained by plotting the moles of triiodide formed at six different exposure time as a function of exposure time (see Figure S5, Electronic Supplementary Material). The rate of formation of triiodide is given by the slope of the calibration curve (47). The rate of triiodide formation in the cuvette is 33 time faster than that in the 96-well plate, consistent with our calculation, within our assumptions and error. No formation of triiodide was observed for unirradiated sample in both cases.

However, on comparing the statistical ratio between the damage constants obtained for the four oligonucleotide targets by these two methods, they are found to be different. TarC and dT_{17} showed a 4-fold increase in the damage constants whereas TarG and TarT showed a 7-fold increase in the value of

their damage constants on switching from the cuvette experiment to the well plate experiment. This difference in the ratio of damage constants can be explained by lower UVC intensity in the well plate experiment and that the 96-well plate samples are unstirred, leading to a slower rate of damage formation. There is also the possibility of secondary photoproduct formation, which may affect the quantum yield and absorption cross-sections, and change the kinetics of photochemical decay. However, the results show that both methods are consistent, and gave a similar pattern of damage constants for all the oligonucleotides.

Conclusion.

We have designed a novel analytical technique to detect DNA damage in a 96-well plate coupled with an automated sample mover. This method has the advantage of irradiating multiple samples in a 96-well plate followed by a fluorescence measurement in a simple mix-and-read assay using smart probes. Thus, we have developed a methodology to examine different damage susceptibilities across multiple oligonucleotide sequences rapidly and efficiently. It is possible to apply this method to construct a library of hot spots which can help in the study of mutagenic mechanism. Although used here for UVC-induced damage, this platform can be used for any environmental or chemical damage agent. The application of this method can be further extended by the use of different probes and well plate of higher density. Thus, this method can be widely used to determine hot spots for DNA damage.

Acknowledgements. This work was supported by a Discovery Grant from the Natural Science and Engineering Research Council of Canada (NSERC) and the Alberta Cancer Board.

References

(1) Marrot, L and Meunier, J. R (2008) Skin DNA photodamage and its biological consequences. *J. Am. Acad. Dermatol.* **58**, S139-S148.

(2) Francesco, L and Horspool, W (Eds) (2003) CRC handbook of Organic Photochemistry and Photobiology . pp.140.1-140.8. CRC Press, USA.

(3) Varghese, A. J and Wang, S. Y (1968) Thymine-thymine adduct as a photoproduct of thymine. *Science.* **160**, 186-187.

(4) Ravanat, J. L., Douki, T and Cadet, J (2001) Direct and indirect effects of UV radiation on DNA and its components. *J. Photochem. Photobiol. B: Biol.* **63**, 88-102.

(5) Douki, T., Perdiz, D., Grof, P., Kuluncsics, Z., Moustacchi, E., Cadet, J and Sage, E (1999) Oxidation of guanine in cellular DNA by solar UV radiation: biological role. *Photochem. Photobiol.* **70**, 184-190.

(6) Schuchert, P., Langsford, M., Kaslin, E and Kohli, J (1991) A specific DNA sequence is required for high frequency of recombination in the *ade6* gene of fission yeast. *EMBO J.* **10**, 2157-2163.

(7) Wahls, W. P and Davidson, M. K (2011) DNA sequence-mediated, evolutionarily rapid redistribution of meiotic recombination hotspots. *Genetics.* **189**, 685-694.

(8) Galtier, N., Enard, D., Radondy, Y., Bazin, E and Belkhir, K (2006) Mutation hot spots in mammalian mitochondrial DNA. *Genome Res*. **16**, 215-222.

(9) Smith, L. E., Denissenko, M. F., Bennett, W. P., Li, H., Amin, S., Tang, M. S and Pfeifer, G.P (2000) Targeting of lung cancer mutational hotspots by polycyclic aromatic hydrocarbans. *J. Natl.Cancer Inst.* **92**, 803-811.

(10) Denissenko, M. F., Chen, J. X., Tang, M. S and Pfeifer, G.P (1997) Cytosine methylation determines hot spots of DNA damage in the human P53 gene. *Proc. Natl. Acad. Sci*. **94**, 3893-3898.

(11) Rogozin, I. B and Pavlov, Y. I (2003) Theoretical analysis of mutation hotspots and their DNA sequence context specificity. *Mutat. Res*. **544**, 65-85.

(12) Hodis, E., Watson, I. R., Kryukov, G. V., Arold, S., Imielinski, M., Theurillat, J., Nickerson, E., Auclair, D., Li, L., Place, C., DiCara, D., Ramos, A. H., Lawrence, M. S., Cibulskis, K., Sivachenko, A., Voet, D., Saksena, G., Stransky, N., Onofrio, R. C., Winckler, W., Ardlie, K., Wagle, N., Wargo, J., Chong, K., Morton, D. L., Hale, K. S., Chen, G., Noble, M., Meyerson, M., Ladbury, J. E., Davies, M. A., Gershenwald, J. E., Wagner, S. N., Hoon, D. S. B., Schadendorf, D., Lander, E. S., Gabriel, S. B., Getz, G., Garraway, L. A and Chin, L (2012) A landscape of driver mutation in melanoma. *Cell*. **150**, 251-263.

(13) Kumar, A., Tyagi, M. B and Jha, P. N (2004) Evidences showing ultraviolet-B radiation-induced damage of DNA in cyanobacteria and its detection by PCR assay. *Biochem. Biophys. Res. Commun*. **318**, 1025-1030.

(14) Rochette, P. J., Bastien, N., Todo, T and Drouin, R (2006) Pyrimidine (6–4) Pyrimidone photoproduct mapping after sublethal UVC doses: nucleotide resolution using terminal transferase-dependent PCR. *Photochem. Photobiol.* **82**, 1370-1376.

(15) Douki, T., Sauvaigo, S., Odin, F and Cadet, J (2000) Formation of the main UV-induced thymine dimeric lesions within isolated and cellular DNA as measured by high performance liquid chromatography-tandem mass spectrometry. *J. Biol. Chem*. **275**, 11678-11685.

(16) Mouret, S., Baudouin, C., Charveron, M., Favier, A., Cadet, J and Douki, T (2006) Cyclobutane pyrimidine dimers are predominant DNA lesions in whole human skin exposed to UVA radiation. *Proc. Natl. Acad. Sci*. **103**, 13765-13770.

(17) Frelon, S., Douki, T and Cadet, J (2002) Radical oxidation of the adenine moiety of nucleoside and DNA: 2-hydroxy-2'-deoxyadenosine is a minor decomposition product. *Free Radic. Res*. **36**, 499-508.

(18) Dizdaroglu, M (1984) The use of capillary gas chromatography-mass spectrometry for identification of radiation-induced DNA base damage and DNA base-amino acid cross-links. *J. Chromatogr. A*. **295**, 103-121.

(19) Slieman, T. A and Nicholson, W. L (2000) Artificial and solar UV radiation induces strand breaks and cyclobutane pyrimidine dimers in Bacillus subtilis spore DNA. *Appl. Environ. Microbiol*. **66**, 199-205.

(20) Weinfeld, M and Soderlind, K. J. M (1991) Phosphorus-32-postlabeling detection of radiation-induced DNA damage: identification and estimation of thymine glycols and phosphoglycolate termini. *Biochemistry*. **30**, 1091-1097.

(21) Kriste, A. G., Martincigh, B. S and Salter, L. F (1996) A sensitive immunoassay technique for thymine dimer quantitation in UV-irradiated DNA. *J. Photochem. Photobiol. A*. **93**, 185-192.

(22) Yarasi, S., McConachie, C and Loppnow, G. R (2005) Molecular beacon probes of photodamage in thymine and uracil oligonucleotides. *Photochem. Photobiol*. **81**, 467-473.

(23) Tyagi, S and Kramer, F. R (1996) Molecular beacons: probes that fluoresce upon hybridization. *Nat. Biotechnol*. **14**, 303-308.

(24) Maksimenko, A., Ishchenko, A. A., Sanz, G., Laval, J., Elder, R. H and Saparbaev, M. K (2004) A molecular beacon assay for measuring base excision repair activities. *Biochem. Biophys. Res. Commun*. **319**, 240-246.

(25) Riches, L. C., Lynch, A. M and Gooderham, N. J (2010) A molecular beacon approach to detecting RAD52 expression in response to DNA damage in human cells. *Toxicol. In Vitro*. **24**, 652-660.

(26) Broude, N. E (2002) Stem-loop oligonucleotides: a robust tool for molecular biology and biotechnology. *Trends Biotechnol*. **20**, 249-256.

(27) Misra, A., Kumar, P and Gupta, K (2007) Design and synthesis of hairpin probe for specific mis-match discrimination. *Nucleic Acids Symp. Ser*. **51**, 311-312.

(28) Tsourkas, A., Behlke, M. A and Bao, G (2002) Structure–function relationships of shared-stem and conventional molecular beacons. *Nucleic Acids Res*. **30**, 4208-4215.

(29) Tsourkas, A., Behlke, M. A., Rose, S. D and Bao, G (2003) Hybridization kinetics and thermodynamics of molecular beacons. *Nucleic Acids Res*. **31**, 1319-1330.

(30) Tan, W., Wang, K and Drake, T. J (2004) Molecular beacons. *Curr. Opin. Chem. Biol*. **8**, 547-553.

(31) El-Yazbi, A.E and Loppnow, G. R (2011) Locked nucleic acid hairpin detection of UV-induced DNA damage. *Can. J. Chem*. **89**, 402-408.

(32) Oladepo, S. A and Loppnow, G. R (2010) The Effect of Tryptophan on UV-induced DNA Photodamage. *Photochem. Photobiol*. **86**, 844-851.

(33) Oladepo, S. A and Loppnow, G. R (2010) Self-quenching smart probes as a platform for the detection of sequence-specific UV-induced DNA photodamage. *Anal. Bioanal. Chem*. **397**, 2949-2957.

(34) Stohr, K., Hafner, B., Nolte, O., Wolfrum, J., Sauer, M and Herten, D. P (2005) Species-specific identification of mycobacterial 16S rRNA PCR amplicons using smart probes. *Anal. Chem*. **77**, 7195-7203.

(35) Maruyama, T., Shinohara, T., Hosogi, T., Ichinose, H., Kamiya, N and Goto, M (2006) Masking oligonucleotides improve sensitivity of mutation detection based on guanine quenching. *Anal. Biochem*. **354**, 8-14.

(36) Knemeyer, J. P and Marme, N., Sauer, M (2000) Probes for detection of specific DNA sequences at the single-molecule level. *Anal. Chem*. **72**, 3717-3724.

(37) Rahn, O. R (1997) Potassium iodide as a chemical actinometer for 254 nm radiation: use of iodate as an electron scavenger. *Photochem. Photobiol*. **66**, 450-455.

(38) El-Yazbi, A. E and Loppnow, G. R (2012) 2-amino purine hairpin probes for the detection of UV-Induced DNA damage. *Anal. Chim. Acta*. **726**, 44-49.

(39) Douki, T and Cadet, J (2001) Individual determination of the yield of the main UV-induced dimeric pyrimidine photoproducts in DNA suggests a high mutagenicity of CC photolesions. *Biochemistry*. **40**, 2495-2501.

(40) Zhang, X., Rosenstein, B. S., Wang, Y., Lebwohl, M., Mitchell, D. M and Wei, H (1997) Induction of 8-Oxo-7, 8-Dihydro-2'-Deoxyguanosine by Ultraviolet Radiation in Calf Thymus DNA and HeLa Cells. *Photochem. Photobiol*. **65**, 119-124.

(41) Smith, C.A and Taylor, J (1993) Preparation and characterization of a set of deoxyoligonucleotide 49-mers containing site-specific cis-syn, trans-syn-I, 96-40, and dewar photoproducts of thymidyly (3′-5′)-thymidine. *J. Biol. Chem*. **15**, 11143-11151.

(42) Oladepo, S. A and Loppnow, G. R (2011) Initial excited-state structural dynamics of 9-methyladenine from UV resonance raman spectroscopy. *J. Phys. Chem. B*. **115**, 6149-6156.

(43) Davies, R. J. H., Malone, J. F., Gan, Y., Cardin, C.J., Lee, M. P. H and Neidle, S (2007) High resolution crystal structure of the intramolecular d(TpA) thymine-adenine photoproduct and its mechanistic implications . *Nucleic Acids Res.* **35**, 1048-1053.

(44) Davies, R. J. H and Sharma, N. D (1989) Extend of formation of a dimeric adenine photoproduct in polynucleotide and DNA. *J. Photochem. Photobiol. B: Biol.* **3**, 247-258

(45) Kurosaki, Y., Abe, H., Morioka, H., Hirayama, J., Ikebuchi, K., Kamo, N., Nikaido, O., Azuma, H and Ikeda, H (2003) Pyrimidine dimer formation and oxidative damage in M13 bacteriophage inactivation by Ultraviolet C irradiation. *Photochem. Photobiol*. **78**, 349-354.

(46) Kundu, L. M., Linne, U., Marahiel, M and Carell, T (2004) RNA is more UV resistant than DNA: The formation of UV-induced DNA lesions is strongly sequence and conformation dependent. *Chem. Eur. J*. **10**, 5697-5705.

(47) Rahn, O. R., Stefan, I. M., Bolton, R. J,. Goren, E., Shaw, S. P and Lykke, R. K (2003) Quantum yeild of the iodide-iodate chemical actinometer: dependence on wavelength and concentration. *Photochem. Photobiol*. **78**, 146-152.

-

Table 1. Oligonucleotides and probes used in this study.

Name	Sequence
TarC	5′-AAA AAA CCA AAA AAA AAA-3′
TarG	5′-AAA AAA AAG GAA AAA AAA-3′
TarT	5′-AAA AAA AAT TAA AAA AAA-3′
dT_{17}	5′-TTT TTT TTT TTT TTT TT-3′
SP_{TarC}	5′-(6-FAM)-CCC CTT TTT TTT TTG GTT TTT TAA GGG G-3′
SP_{TarG}	5′-(6-FAM)-CCC CTA ATT TTT TTT CCT TTT TTT TAG GGG-3′
SP_{TarT}	5′-(6-FAM)-CCA CAA TTT TTT TTA ATT TTT TTT GTG G-3′
SP_{dT17}	5′-(6-FAM)-CCC AAA AAA AAA AAA AAA AAT TGG G-3′
MB_{dT17}	5′-(6-FAM)-CAC TTT AAA AAA AAA AAA AAA AAG TG-(3DAB)-3′

Oligonucleotide target sequences and probe sequences used in this study. 5′-Fluorescein (6-FAM) is the fluorophore attached at the 5′-end for both MB and SPs, and 3′-dabcyl (3DAB) is the dark fluorescence quencher attached to the 3′-end of the MB only. The underlined bases in the sequence of MB and SPs are the bases that form the stem, and the underlined bases in the targets are the nominal site of damage.

Table 2. UVC damage constants obtained for the 4 different DNA target sequences.

Name	96 well plate experiment τ (min)		Average τ (min)	Cuvette Experiment τ (min)
	1	2		
TarC	130 ± 20	130 ± 30	130 ± 40	30 ± 2
TarG	60 ± 10	60 ± 9	60 ± 10	8 ± 1
TarT	100 ± 10	85 ± 6	90 ± 10	15 ± 3
dT_{17}	11 ± 0.4	13 ± 0.6	12 ± 0.7	3.8 ± 0.1

Damage constants obtained for the four oligonucleotide sequences used in this work. The values were obtained from the fluorescence damage curves which were fit to a single exponential function.

Figure Captions:

Figure 1. Melting curve of 0.18 μM SP alone (filled squares), 0.18 μM SP in the presence of a 3-fold excess of perfectly complementary undamaged oligonucleotide target (filled triangles) and 0.18 μM SP in the presence of a 3-fold excess of complementary damaged oligonucleotide target (open circles). The different panels represent the melting curves for (A) SP_{TarC}, (B) SP_{TarG}, and (C) SP_{TarT}. Fluorescence curves have each been scaled to the SP alone.

Figure 2. Melting curve of 0.53 μM SP_{dT17} alone (filled squares), 0.18 μM SP_{dT17} in the presence of a 3-fold excess of perfectly complementary oligonucleotide target (filled triangles) and 0.18 μM SP_{dT17} in the presence of a 3-fold excess of complementary oligonucleotide damaged for 9 min (filled circles), 25 min (open triangles) and 57 min (open circles). Fluorescence curves have each been scaled to the SP_{dT17} alone.

Figure 3. Fluorescence decay curves for (A) MB and (B) SP detection of damage in dT_{17} in the 96-well plate. The curve were obtained by exciting the hybridization mixture of 0.53 μM target and 0.18 μM complementary SP_{dT17} or MB_{dT17} in buffer (5 mM $MgCl_2$, 20 mM NaCl, 10 mM Tris and 1 mM EDTA, pH 7.4) at 480 nm and emission recorded at 520 nm. The solid lines through the points are single exponential $I_F = I_o + Ae^{-t/\tau}$ fits. The fluorescence parameters obtained from the fit for dT_{17} with MB probe are I_o = 0.84 ± 0.02 x 10^3 cps, A = 5.32 ± 0.37 x 10^3 cps and τ_1 = 6.90 ± 0.70 min. The

fluorescence parameters obtained from the fit for dT_{17} with SP probe are I_o = 3.46 ± 0.07 x 10^3 cps, A = 2.31 ± 0.21 x 10^3 cps and τ_1 = 10.72 ± 1.28 min.

Figure 4. SP_{dT17}-target hybrid fluorescence intensity at 520 nm as a function of calculated photoproduct formation in a 0.18 μM solution of dT_{17} in a cuvette. Inset shows the linear portion of the graph with R^2 = 0.96. The sensitivity (slope of the calibration curve) is 4.0 x 10^{11} M^{-1}. LOD and LOQ values are 55 nM and 183 nM, respectively.

Figure 5. Fluorescence damage curve for (A) TarC, (B) TarG, (C) TarT and (D) dT_{17}. Graphs were obtained by exciting the hybridization mixture of 0.53 μM target and 0.18 μM SP_{TarC} in Tris buffer at 480 nm and recording the emission at 520 nm. The solid lines through the points are single exponential $I_F = I_o + Ae^{-t/\tau}$ fits. The fluorescence parameters obtained from the fit for TarC are I_o = 2.08 ± 0.39 x 10^3 cps, A = 4.20 ± 0.31 x 10^3 cps and τ_1 = 130 ± 30 min. The fluorescence parameter obtained for sequences TarG are I_o = 2.71 ± 0.12 x 10^3 cps, A = 3.36 ± 0.14 x 10^3 cps and τ_1 = 60 ± 9 min. The fluorescence parameter obtained for sequences TarT are I_o = 2.66 ± 0.06 x 10^3 cps, A = 3.06 ± 0.06 x 10^3 cps and τ_1 = 85 ± 6 min. The fluorescence parameters obtained for sequences dT_{17} are I_o = 4.69 ± 0.01 x 10^3 cps, A = 1.70 ± 0.03 x 10^3 cps and τ_1 = 13 ± 0.6 min.

Multiplexed, UVC-Induced, Sequence-Dependent DNA Damage Detection

Supplementary Material

Sindhu G. Nair and Glen R. Loppnow*

Department of Chemistry, University of Alberta,

Edmonton, Alberta T6G 2G2 Canada

Table S1. Fluorescence intensity of blank sample.

Fluorescence Intensity (x 10^5 cps)
4.7
4.6
4.8
4.8
4.6
4.7
4.6
4.6
4.7
4.7
4.6
4.8
4.8
4.6
4.7
4.5
4.7
4.6
Avg ± SD 4.7 ± 0.07

Fluorescence intensity for 0.18 μM SP_{dT17} in buffer. 'Avg' is average and 'SD' is standard deviation. These values were used for calculating the LOD and LOQ.

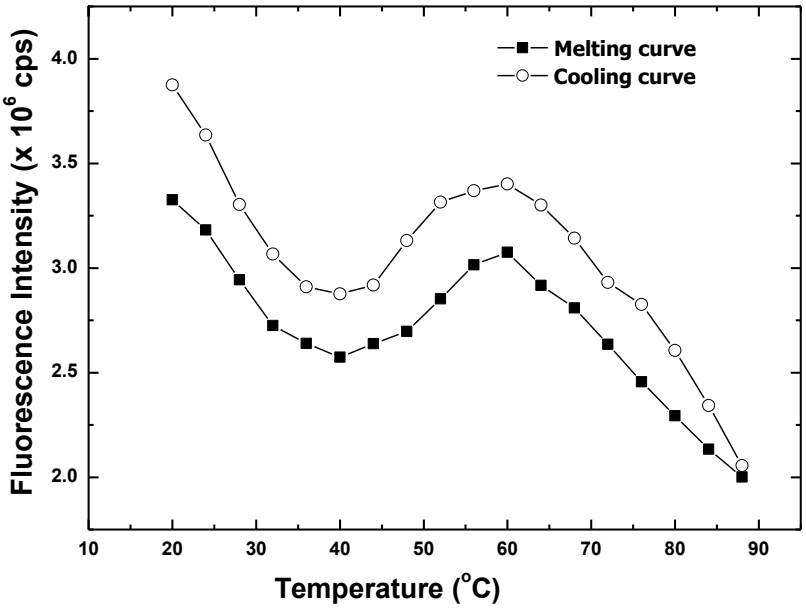

Figure S1. Melting (filled squares) and cooling curve (open circles) of 0.18 μM SP_{TarC} alone. The melting curve was generated at a heating rate of 1°C/min, in 4°C increments and with a 5 min holding time after each increment. The cooling curve was performed with all the above conditions, except -4°C increments were used.

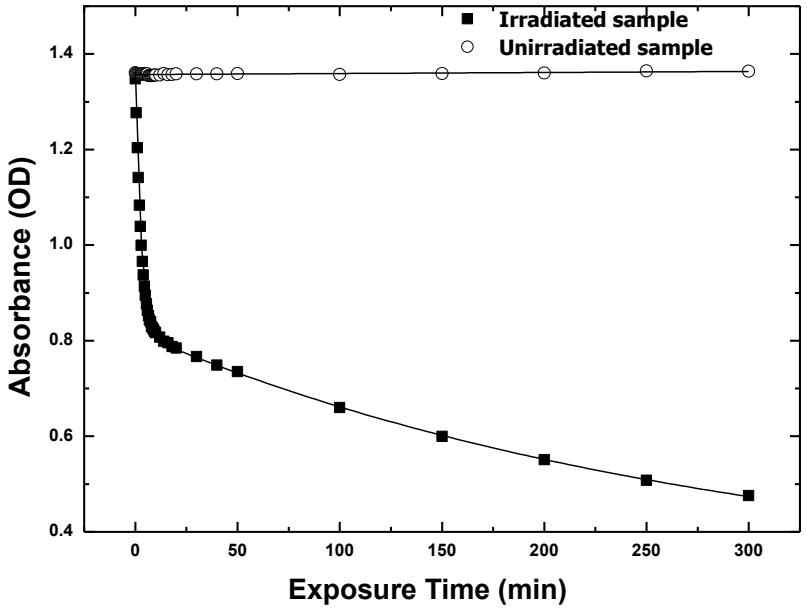

Figure S2. Absorbance at 260 nm as a function of UVC exposure time for a 10 μM dT_{17} irradiated sample (filled squares) and 10 μM unirradiated dT_{17} control (open circles). The solid line through the filled squares is fit to a double exponential function, $A = A_0 + C_1 e^{-t/\tau_1} + C_2 e^{-t/\tau_2}$. The absorbance parameter obtained from the fit are C_1 = 0.81 OD, C_2 = 0.53 OD, A_0= 0.29 OD, τ_1 = 2.79 ± 0.04 min, τ_2 = 288.46 ± 41.43 min. The solid line through the open circles is fit to a straight line of zero slope by eye.

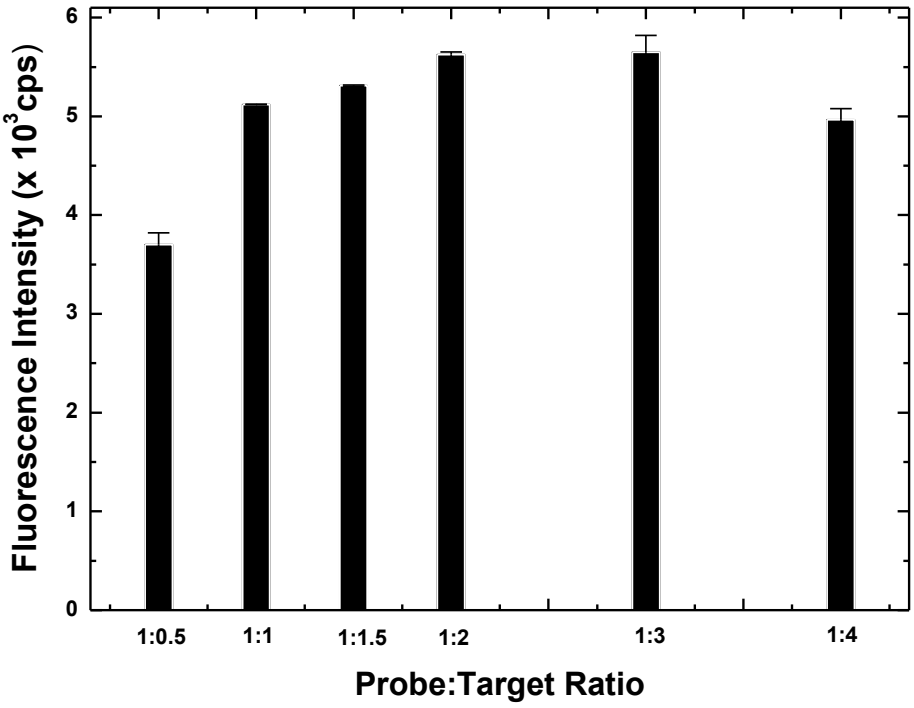

Figure S3. Fluorescence intensities for different ratios of SP_{TarC}:TarC. Different ratios are obtained by keeping the concentration of SP constant at 0.18 μM and varying the concentration of target.

-

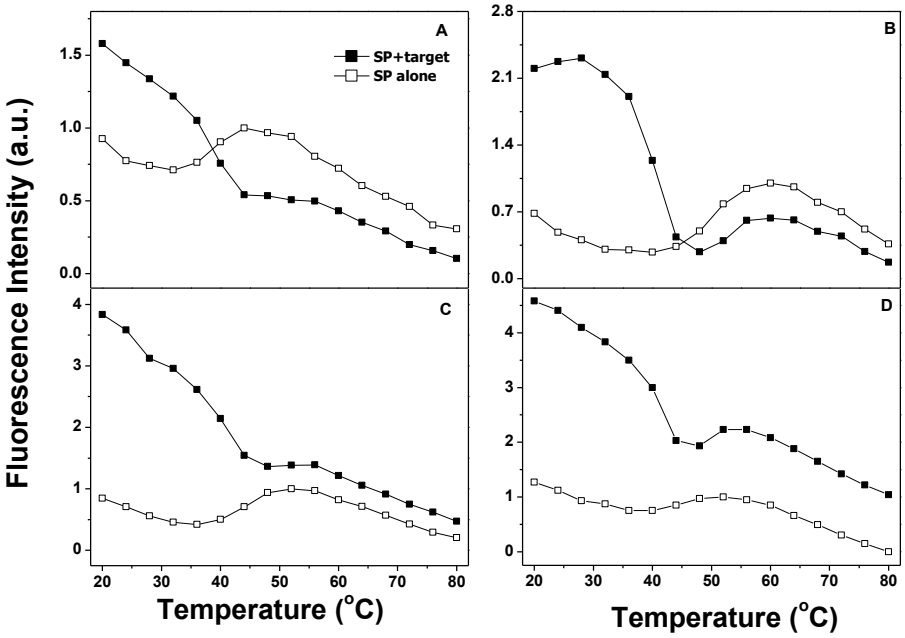

Figure S4. Melting curves of 0.18 μM SP alone (open circles) and 0.18 μM SP in the presence of a 3-fold excess of perfectly complementary oligonucleotide target sequence (filled squares) in 10mM Tris and 1mM EDTA with varying Na^+ and Mg^{2+} concentrations. The melting curves use (A) 1 mM $MgCl_2$, (B) 3 mM $MgCl_2$, (C) 3 mM $MgCl_2$ and 20 mM NaCl and (D) 5 mM $MgCl_2$ and 20 mM NaCl. Fluorescence curves have each been scaled to SP alone.

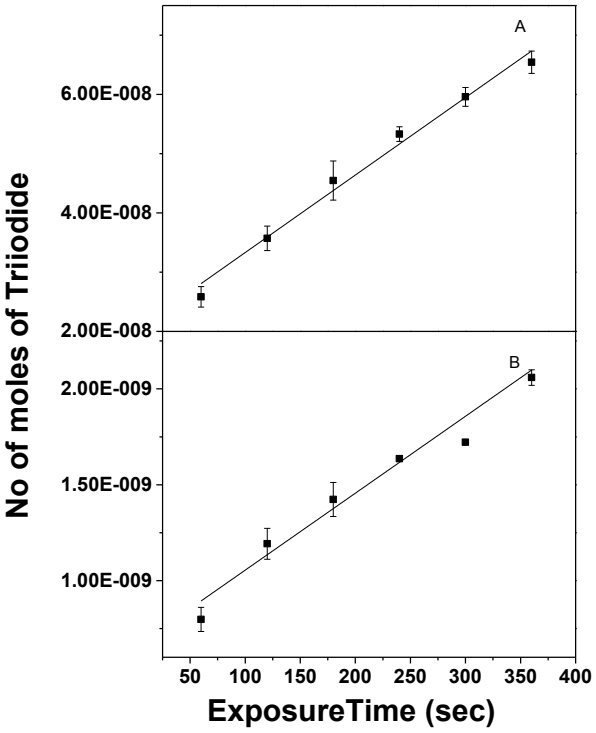

Figure S 5. Moles of triiodide formed as a function of exposure time for (A) Cuvette method and (B) Well plate method. The solid line through the points are linear fit with slope of the calibration curve for cuvette method = 1.31 x 10^{-10} mol.s^{1}and well plate method = 4.01 x 10^{-12} mol.s^{-1} respectively.